A model-free Data-Driven paradigm for *in situ* patient-specific prediction of human brain response to ultrasound stimulation

Hossein Salahshoor[1], Michael Ortiz[1,*]

1 Division of Engineering and Applied Science, California Institute of Technology, 1200 E California Blvd, Pasadena, CA 91125

*** ortiz@caltech.edu**

Abstract

We present a class of model-free Data-Driven solvers that effectively enable the utilization of *in situ* and *in vivo* imaging data *directly* in full-scale calculations of the mechanical response of the human brain to ultrasound stimulation, entirely bypassing the need for analytical modeling or regression of the data. We demonstrate the approach, including its ability to make detailed spatially-resolved patient-specific predictions of wave patterns, using public-domain MRI images, MRE data and commercially available solid-mechanics software.

Significance statement

Accurate patient-specific computational models of wave propagation in the human brain are fundamental for understanding the complex wave patterns induced by ultrasound (US) stimulation with a view to improving and optimizing clinical procedures. A critical bottleneck in the predictive ability of computational models has been the complexity, paucity of data and observational uncertainty pertaining to the mechanical behavior of brain tissue, both healthy and diseased. Recent developments of advanced microscopy methods, such as Magnetic Resonance Elastography (MRE) enable the *in situ* and *in vivo* characterization of the viscoelastic response of the brain tissue of individual patients in a clinical environment. We develop a new model-free Data-Driven framework that directly incorporates patient-specific data on-the-fly into calculations of wave patterns in the brain resulting from US stimulation. We demonstrate the framework by performing full-scale spatially-resolved calculations based on public domain viscoelastic data from MRE measurements.

Introduction

Predictive modeling of the mechanical response of the human brain to ultrasound stimulation is an important part of many preventive, diagnostic, and therapeutic biomedical procedures [2,14,18,19]. Computational models are increasingly incorporated to inform or guide biomedical research such as transcranial ultrasound stimulation therapies. However, the efficacy of such models depends crucially on precise patient-specific representations of both the geometry and the material response of the brain *in vivo* [5,13,21].

In contrast to recent advances in high-resolution, patient-specific, *in-vivo*, and non-invasive imaging techniques, which presently enable accurate representations of

brain anatomy down to ultra-fine features [7,8], the accurate and reliable material modeling of brain tissue has proven challenging and remains a major predictive bottleneck [3,4]. These modeling challenges arise from the ultra-compliant, complex, heterogeneous, and patient-specific nature of the mechanical properties of brain tissue [3]. These complexities cannot easily be reduced to analytical formulas that differentiate, e.g., between healthy and diseased tissue and the presence of tumors and other lesions in a particular patient.

By way of contrast, recent advances in microscopy and elastography techniques, such as Magnetic Resonance Elastography (MRE) [12], have made possible the *in vivo* characterization of the viscoelastic response of brain tissue in individual patients. Indeed, MRE technology presently allows personalized atlases of brain-tissue viscoelastic properties, including storage and loss moduli as functions of frequency, to be compiled *in vivo* [1,9]. These advances have radically transformed brain biomechanics from a data-starved to a data-rich field, a transformation that challenges theory and computational practice in fundamental and far-reaching ways.

Several possible strategies can be pursued in response to these challenges and opportunities. One currently popular strategy uses Machine Learning (ML) regression in order to fit the data, e.g., using neural-network representations [22]. However, any method of regression, whether based on neural networks or on some other functional representation, is necessarily *lossy*. Indeed, regression replaces the empirical data set by a fitted function, a process that inevitably results in loss of information, biases and uncontrolled modeling errors. In addition, models need to be trained *in situ* for specific patients, which is costly and time consuming.

An appealing alternative is to formulate solvers that effectively enable the utilization of *in situ* and *in vivo* imaging data *directly* in calculations, thus entirely bypassing the intermediate material modeling step. In this work, we demonstrate how one such model-free Data-Driven paradigm [17] can be used to forge a direct connection between *in situ* and *in vivo* patient-specific measurements of viscoelastic brain-tissue properties and real-time full-scale calculations of the mechanical response of the human brain to ultrasound stimulation, cf. Section 1. For purposes of demonstration and verification, we specifically use a public-domain MRE data set [9] and the corresponding MNI stereotaxic space to develop a finite-element model of the human brain co-registered with the voxel-based MRE data. We then use our model-free Data-Driven solver [17] to compute, directly from the data, wave patterns in the brain resulting from transcranial ultrasound stimulation, cf. Section 2.

The model-free Data-Driven approach demonstrated in this paper suggests a natural path for achieving on-the-fly patient-specific predictions of brain mechanics in a clinical environment. We illustrate the patient-specific aspect of our model-free Data-Driven brain approach by considering MRE data sets from eight different healthy human subjects from the repository provided by [9]. The computed shear strain amplitudes exhibit variations of up to 25%, which, as expected, bears out the need for patient-specific predictions.

We anticipate that strictly Data-Driven approaches such as demonstrated here will supply a valuable basis for developing and optimizing patient-specific therapeutic procedures in the future.

1 Data-Driven brain mechanics

A schematic of the proposed model-free Data-Driven framework is shown in Fig. 1. We use anatomical data, in the form of MRI images, Fig. 1 top-left, in conjunction with a co-registered atlas of viscoleastic properties of the brain tissue, Fig. 1 bottom-left, to generate a finite-element model of the brain, Fig. 1 top-right. We choose the

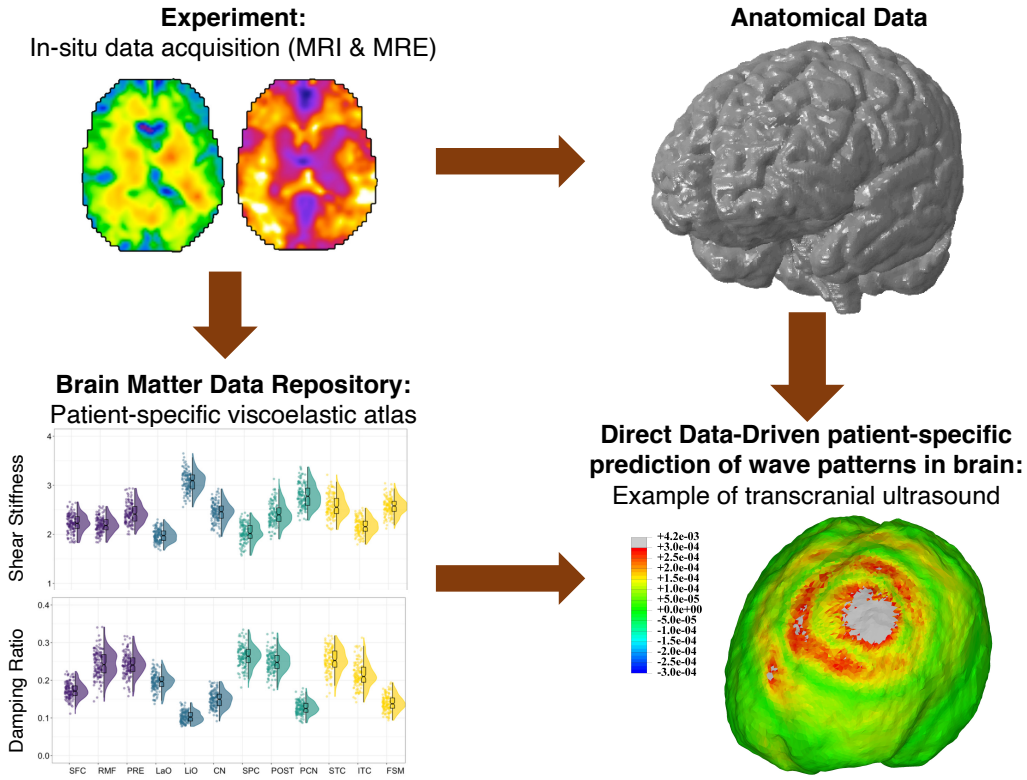

Figure 1. Schematic of the model-free Data-Driven brain mechanics paradigm. Top-left: anatomical data in the form of MRI images. Bottom-left: co-registered atlas of viscoleastic properties of the brain tissue. Top-right: finite-element model of the brain. Bottom-right: steady-state wave pattern induced by low-intensity focus ultrasound (LIFUS) applied to a region on the frontal lobe.

finite-element mesh size equal to, or smaller than, the voxel size in the MRE atlas, so that every material point in the mesh can be assigned to a unique MRE voxel. The bone tissue is assumed to be linear elastic. We then solve in the frequency domain for the steady-state wave pattern induced by low-intensity focus ultrasound (LIFUS) applied to a region on the frontal lobe, Fig. 1 bottom-right. Specifically, the Data-Driven solver endeavors to minimize the discrepancy between local material states in the finite-element model and the MRE data while simultaneously enforcing dynamic equilibrium in the sense of the Helmholtz equation. Conveniently, the solver can be implemented as a wrapper around conventional FE element programs, including commercially available software. A complete mathematical description of the Data-Driven solver and an assessment of convergence with respect to the data may be found [17].

2 Predicting wave patterns in transcranial ultrasound stimulation

We demonstrate the range and scope of the model-free Data-Driven brain mechanics framework through an application to transcranial ultrasound stimulation. Transcranial ultrasound has elicited growing interest in both low-intensity mode, suited to neuromodulation applications [2,10,14–16,18–20], as well as in high-intensity mode,

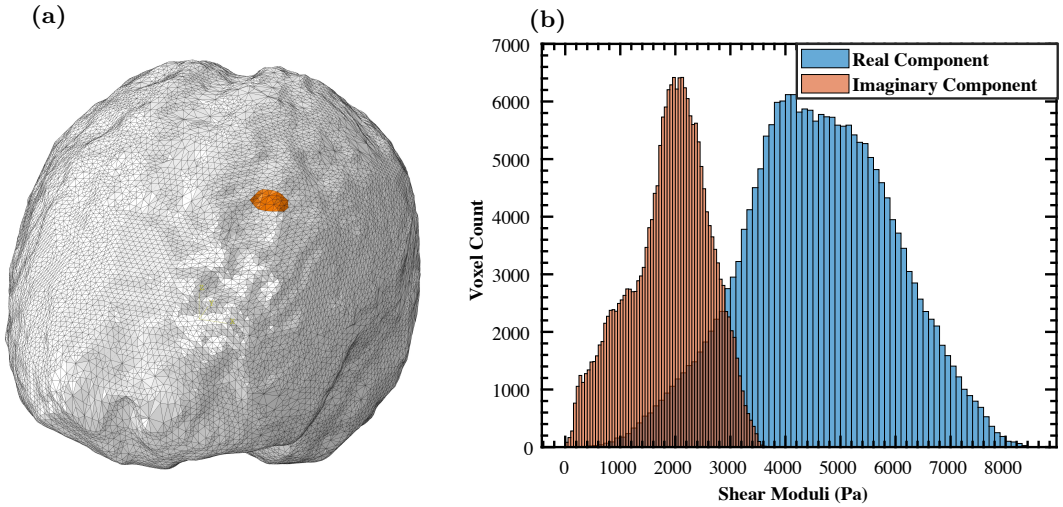

Figure 2. (A): Finite element model of a heterogeneous brain with 0.2 million tetrahedral elements. Transcranial ultrasound stimulation is modeled by subjecting the highlighted region to ultrasound pressure as a traction boundary condition. (B): histogram of complex shear moduli from MRE data. The computational model is co-registered to the data. Both the geometry and viscoelastic map are obtained from public domain MRE data [9].

germane to tumor ablation applications [11, 23].

For purposes of demonstration, we use the recently published atlas of viscoelastic properties of brain tissue [9], acquired at a single frequency of 50 Hz from 134 human subjects. We also adopt the associated MNI coordinate data to develop a computational heterogeneous brain model, co-registered to the MRE data. The resultant geometry is discretized into a finite element model comprising 0.2 million three-dimensional tetrahedral elements, Fig. 2a. We note that the MRE data encodes complex viscoelastic shear moduli with real and imaginary components, corresponding to storage and loss moduli for each material point, respectively. For the sake of simplicity, we assume the brain matter to be isotropic, with an elastic bulk modulus of 2 GPa assigned to the entire model. We remark that, conditioned on the availability of the data, the present framework can account for fully anisotropic brain matter or other material symmetries thereof. Fig. 2b shows a histogram of the complex moduli in the material data set binned by voxel. The wide spread of properties in the material data set resulting from material heterogeneity, patient-to-patient variability and measurement scatter is noteworthy.

We subject a small region on the frontal lobe of the brain, shown in orange in Fig. 2, to a sinusoidal pressure with a peak amplitude of 60 kPa. Calculations were performed using the commercial finite-element software Abaqus (Abaqus/Standard, Dassault Systemes Simulia, France) as compute engine within the model-free Data-Driven wrapper. Fig. 3 shows computed contours of the real and imaginary components of all six components of the strain tensor across the entire brain. The relatively higher magnitude of the shear strains with respect to volumetric strains is expected from the softness of the brain tissue in shear. The relative ease of implementation of the framework on top of readily available commercial software and the speed of the calculations, comparable to that of a simple elastic analysis, are also noteworthy.

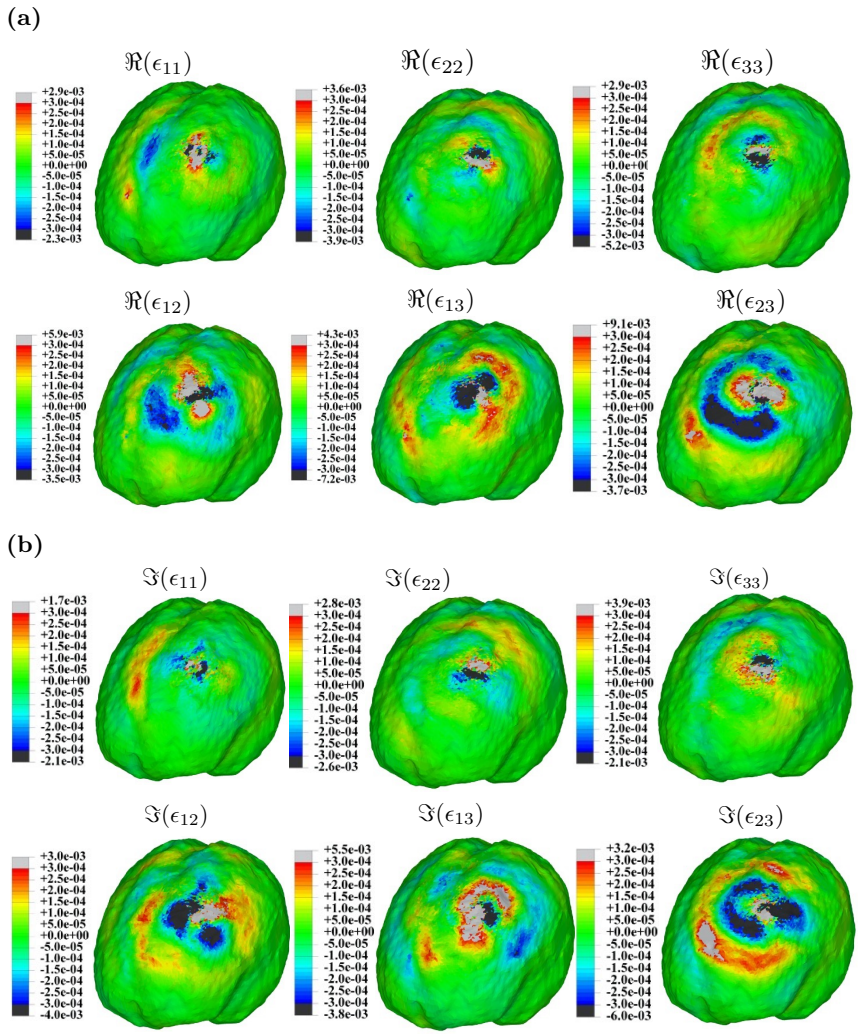

Figure 3. Model-free Data-Driven simulation of transcranial ultrasound stimulation on a region on the frontal lobe of brain, Fig. 2a. Spatial distribution of components of strain at steady state. a) Real part; b) Imaginary part.

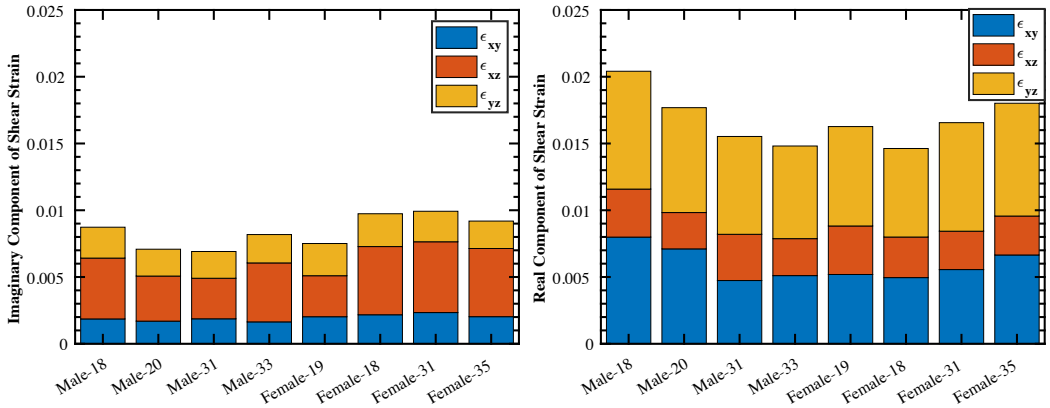

Figure 4. Model-free Data-Driven simulation of transcranial ultrasound stimulation on a region on the frontal lobe of brain, Fig. 2a, for eight patient-specific MRE data sets. Maximum strain amplitudes at steady state. Left: Imaginary part; Right: Real part.

3 Patient-specific modeling

We illustrate the patient-specific aspect of our model-free Data-Driven brain approach by considering MRE data sets from eight different healthy human subjects from the repository provided by [9]. The subjects were four male and four female with ages varying from 18 to 35. As in the preceding section, we solve the corresponding eight Data-Driven problems of transcranial ultrasound stimulation with all components of the computational model held fixed except for the complex moduli data. Histograms of the material data set binned by voxel for all eight patients are depicted in the supplementary file. We again emphasize that all calculations are based directly on the MRE data without recourse to analytical modeling of the data at any stage of the calculations.

Fig. 4 shows the computed maximum complex amplitude of harmonic shear strains at a frequency of 50 Hz for all eight patients. The appendix contains the computed contours of real and imaginary components of both maximum and minimum principal strain across the entire brain for all eight patients. We observe that the real component of maximum shear strain ϵ_{xy} varies from 0.015 to 0.021, or a 25% spread, with similar variations for the remaining components. As expected, these results bear out the importance of patient-specific data and illustrate the potential of model-free Data-Driven methods for achieving patient specificity on demand in a clinical environment.

Materials and Methods

A detailed summary of the method in presented in the SI Appendix. The model-free Data-Driven solver strives to find admissible states of stress and strain in the finite-element model that are closest to the material data set in the sense of a suitable measure of discrepancy [17]. The finite-element model supplies a representation of the geometry of the brain, which is assumed to be free-standing, and the ultrasound pressure loading applied to it. It also provides a means of enforcing admissibility of the fields, i. e., strain compatibility and stress equilibrium. The material behavior of the brain tissue is assumed to be linear viscoelastic. The problem of wave propagation is formulated in the frequency domain and is governed by the complex Helmholtz equation.

The viscoelastic behavior of the brain tissue is characterized by empirical data sampling the dependence of the complex modulus on frequency. The data may be noisy owing to measurement error and experimental scatter. The discrepancy between finite-element stress and strain field and the material data is minimized iteratively. The requisite finite-element calculations are conducted using the commercial code Abaqus (Abaqus/Standard, Dassault Systemes Simulia, France). A detailed analysis of the well-posedness of the method and convergence with respect to data is presented in [6] for the elastic case.

Data availability

The data that support the findings of this study are available within this article and references therein. The simulation protocols are also available from the corresponding author upon request.

Acknowlegments

This project was supported by U.S. National Institutes of Health Grant No. 1RF1MH117080.

References

1. P. V. Bayly, A. Alshareef, A. K. Knutsen, K. Upadhyay, R. J. Okamoto, A. Carass, J. A. Butman, D. L. Pham, J. L. Prince, K. Ramesh, et al. Mr imaging of human brain mechanics in vivo: new measurements to facilitate the development of computational models of brain injury. *Annals of biomedical engineering*, 49(10):2677–2692, 2021.

2. J. Blackmore, S. Shrivastava, J. Sallet, C. R. Butler, and R. O. Cleveland. Ultrasound neuromodulation: a review of results, mechanisms and safety. *Ultrasound in medicine & biology*, 45(7):1509–1536, 2019.

3. S. Budday, T. C. Ovaert, G. A. Holzapfel, P. Steinmann, and E. Kuhl. Fifty shades of brain: a review on the mechanical testing and modeling of brain tissue. *Archives of Computational Methods in Engineering*, 27(4):1187–1230, 2020.

4. S. Chatelin, A. Constantinesco, and R. Willinger. Fifty years of brain tissue mechanical testing: from in vitro to in vivo investigations. *Biorheology*, 47(5-6):255–276, 2010.

5. A. Chaturvedi, C. R. Butson, S. F. Lempka, S. E. Cooper, and C. C. McIntyre. Patient-specific models of deep brain stimulation: influence of field model complexity on neural activation predictions. *Brain stimulation*, 3(2):65–77, 2010.

6. S. Conti, S. Müller, and M. Ortiz. Data-driven problems in elasticity. *Archive for Rational Mechanics and Analysis*, 229:79–123, 2018.

7. A. M. Dale, A. K. Liu, B. R. Fischl, R. L. Buckner, J. W. Belliveau, J. D. Lewine, and E. Halgren. Dynamic statistical parametric mapping: combining fmri and meg for high-resolution imaging of cortical activity. *neuron*, 26(1):55–67, 2000.

8. C. Errico, J. Pierre, S. Pezet, Y. Desailly, Z. Lenkei, O. Couture, and M. Tanter. Ultrafast ultrasound localization microscopy for deep super-resolution vascular imaging. *Nature*, 527(7579):499–502, 2015.

9. L. V. Hiscox, M. D. McGarry, H. Schwarb, E. E. Van Houten, R. T. Pohlig, N. Roberts, G. R. Huesmann, A. Z. Burzynska, B. P. Sutton, C. H. Hillman, et al. Standard-space atlas of the viscoelastic properties of the human brain. *Human brain mapping*, 41(18):5282–5300, 2020.

10. A. Jerusalem, Z. Al-Rekabi, H. Chen, A. Ercole, M. Malboubi, M. Tamayo-Elizalde, L. Verhagen, and S. Contera. Electrophysiological-mechanical coupling in the neuronal membrane and its role in ultrasound neuromodulation and general anaesthesia. *Acta biomaterialia*, 2019.

11. G. Mauri, L. Nicosia, Z. Xu, S. Di Pietro, L. Monfardini, G. Bonomo, G. M. Varano, F. Prada, P. Della Vigna, and F. Orsi. Focused ultrasound: tumour ablation and its potential to enhance immunological therapy to cancer. *The British journal of radiology*, 91(xxxx):20170641, 2018.

12. R. Muthupillai, D. Lomas, P. Rossman, J. F. Greenleaf, A. Manduca, and R. L. Ehman. Magnetic resonance elastography by direct visualization of propagating acoustic strain waves. *science*, 269(5232):1854–1857, 1995.

13. M. L. Neal and R. Kerckhoffs. Current progress in patient-specific modeling. *Briefings in bioinformatics*, 11(1):111–126, 2010.

14. C. Rabut, S. Yoo, R. C. Hurt, Z. Jin, H. Li, H. Guo, B. Ling, and M. G. Shapiro. Ultrasound technologies for imaging and modulating neural activity. *Neuron*, 108(1):93–110, 2020.

15. J. L. Robertson, B. T. Cox, J. Jaros, and B. E. Treeby. Accurate simulation of transcranial ultrasound propagation for ultrasonic neuromodulation and stimulation. *The Journal of the Acoustical Society of America*, 141(3):1726–1738, 2017.

16. H. Salahshoor, H. Guo, M. G. Shapiro, and M. Ortiz. Mechanics of ultrasonic neuromodulation in a mouse subject. *Extreme Mechanics Letters*, 50:101539, 2022.

17. H. Salahshoor and M. Ortiz. Model-free data-driven viscoelasticity in the frequency domain. *arXiv preprint arXiv:2205.06674*, 2022.

18. H. Salahshoor, M. G. Shapiro, and M. Ortiz. Transcranial focused ultrasound generates skull-conducted shear waves: Computational model and implications for neuromodulation. *Applied Physics Letters*, 117(3):033702, 2020.

19. T. Sato, M. G. Shapiro, and D. Y. Tsao. Ultrasonic neuromodulation causes widespread cortical activation via an indirect auditory mechanism. *Neuron*, 98(5):1031–1041, 2018.

20. W. J. Tyler. Noninvasive neuromodulation with ultrasound? a continuum mechanics hypothesis. *The Neuroscientist*, 17(1):25–36, 2011.

21. A. Wittek, K. Miller, R. Kikinis, and S. K. Warfield. Patient-specific model of brain deformation: Application to medical image registration. *Journal of biomechanics*, 40(4):919–929, 2007.

22. K. Xu, A. M. Tartakovsky, J. Burghardt, and E. Darve. Learning viscoelasticity models from indirect data using deep neural networks. *Computer Methods in Applied Mechanics and Engineering*, 387:114124, 2021.

23. Y.-F. Zhou. High intensity focused ultrasound in clinical tumor ablation. *World journal of clinical oncology*, 2(1):8, 2011.

Supporting Information Text

Data-driven viscoelasticity in the frequency domain

For completeness and ease of reference, we summarize the equations that govern the calculations of brain ultrasound stimulation presented in this work. Further detail of the formulation and the solver can be found in [17].

We consider a finite-element model of the brain containing n nodes and m material points. The state of the brain at time t is characterized by strains $\epsilon(t) \equiv \{\epsilon_e(t) \in \mathbb{R}^d,\ e = 1, \dots, m\}$ and stresses $\sigma(t) \equiv \{\sigma_e(t) \in \mathbb{R}^d,\ e = 1, \dots, m\}$, where d is the stress and strain dimension, subject to compatibility and dynamic equilibrium constraints of the form

$$\epsilon_e(t) = B_e u(t) + g_e(t), \quad e = 1, \dots m, \tag{1a}$$

$$M\ddot{u}(t) + \sum_{e=1}^{m} w_e B_e^T \sigma_e(t) = f(t), \tag{1b}$$

where $u(t) \in \mathbb{R}^n$ is the array of unconstrained nodal displacements at time t, with n the spatial dimension, $f(t) \in \mathbb{R}^n$ is a nodal force array at time t, $g_e(t) \in \mathbb{R}^d$ is an initial strain at time t resulting from prescribed displacement boundary conditions, w_e are positive weights, $B_e \in L(\mathbb{R}^n, \mathbb{R}^d)$ is the strain-displacement matrix for material point e and $M \in \mathbb{R}^{n\times n}$ is a mass matrix.

The governing equations (1) can also be expressed in compact matrix form as

$$\epsilon(t) = Bu(t) + g(t), \tag{2a}$$

$$M\ddot{u}(t) + B^T W \sigma(t) = f(t) \tag{2b}$$

with $B = (B_1, \dots, B_m) \in \mathbb{R}^{N\times n}$, $N = md$, $\epsilon(t) = (\epsilon_1(t), \dots, \epsilon_m(t)) \in \mathbb{R}^N$, $g(t) = (g_1(t), \dots, g_m(t)) \in \mathbb{R}^N$, $\sigma(t) = (\sigma_1(t), \dots, \sigma_m(t)) \in \mathbb{R}^N$ and $W \in \mathbb{R}^{N\times N}$ is a diagonal matrix of weights such that $W\sigma = \{w_1\sigma_1, \dots, w_m\sigma_m\}$.

An application of the Fourier transform to (2) gives

$$\hat{\epsilon}(\omega) = B\hat{u}(\omega) + \hat{g}(\omega), \tag{3a}$$

$$B^T W \hat{\sigma}(\omega) - M\omega^2 \hat{u}(\omega) = \hat{f}(\omega), \tag{3b}$$

where $(\hat{\ })$ denotes the Fourier transform of a function and ω is the frequency. We note that the Fourier transform of a harmonic time history is a Dirac measure centered at the harmonic frequency. Therefore, in general the relations (3) must be interpreted in the sense of measures.

At every material point e, linear viscoelasticity is characterized as a linear *hereditary law* of the form

$$\sigma_e(t) = \int_{-\infty}^{t} \mathbb{J}_e(t-s)\, \dot{\epsilon}_e(s)\, ds = (\mathbb{J}_e * \dot{\epsilon}_e)(t), \tag{4}$$

where $\mathbb{J}_e : [0, +\infty) \to L(\mathbb{R}^{d\times d}_{\text{sym}}, \mathbb{R}^{d\times d}_{\text{sym}})$, $\mathbb{J}_e^T(t) = \mathbb{J}_e(t)$, $\mathbb{J}_e(t)$ to 0 for $t < 0$, is the relaxation function and $*$ is the convolution operator. We may regard (4) as a mapping that gives the stress $\sigma(t)$ and time t as a function of the past history of strain.

Taking the Fourier transform of (4) and applying the convolution theorem, we obtain

$$\hat{\sigma}_e(\omega) = i\omega \hat{\mathbb{J}}_e(\omega)\hat{\epsilon}_e(\omega) \equiv \mathbb{E}(\omega)\hat{\epsilon}_e(\omega), \tag{5}$$

where $\mathbb{E}(\omega) = \mathbb{E}'(\omega) + i\mathbb{E}''(\omega)$ is the complex modulus and

$$\mathbb{E}'(\omega) = \omega \int_0^\infty \mathbb{J}(s) \sin(\omega s)\, ds, \tag{6a}$$

$$\mathbb{E}''(\omega) = \omega \int_0^\infty \mathbb{J}(s) \cos(\omega s)\, ds, \tag{6b}$$

are the storage and loss moduli, respectively.

If, as in the case of ultrasound stimulation at steady state, the forcing is harmonic, we specifically have

$$\hat{f} = 2\pi F \delta_\Omega, \quad \hat{g} = 2\pi G \delta_\Omega, \tag{7}$$

where $F \in \mathbb{C}^n$ and $G \in \mathbb{C}^N$ are constant complex amplitudes, Ω is the transduction frequency and δ_a denotes the Dirac delta centered at a. In this particular case, (3) is solved by setting

$$\hat{u} = 2\pi U \delta_\Omega, \quad \hat{\epsilon} = 2\pi E \delta_\Omega, \quad \hat{\sigma} = 2\pi S \delta_\Omega, \tag{8}$$

with constant complex amplitudes $U \in \mathbb{C}^n$, $E \in \mathbb{C}^N$ and $S \in \mathbb{C}^N$ such that

$$E = BU + G, \tag{9a}$$

$$B^T W S - M\Omega^2 U = F. \tag{9b}$$

Suppose that the complex modulus $\mathbb{E}(\Omega)$ of the material is known exactly. Then,

$$S = \mathbb{E}(\Omega)\, E, \tag{10}$$

which, together with (Js6jNy), determines the unknown amplitudes $U \in \mathbb{C}^n$, $E \in \mathbb{C}^N$ and $S \in \mathbb{C}^N$.

An alternative formulation that provides a basis for the Data-Driven approach is the following. Let $\mathcal{Z}$ be the phase space of all harmonic histories $(\epsilon(t), \sigma(t))$. We may then regard the local constitutive relation (4), or its Fourier representation (5), as restricting the possible histories to a material set

$$\mathcal{D} = \{(\epsilon(t), \sigma(t)) \in \mathcal{Z} \,:\, \text{eq. (4) or eq. (5)}\}. \tag{11}$$

Likewise, we may regard (2), or its Fourier representation (3) as defining a constraint set of admissible histories

$$\mathcal{E} = \{(\epsilon(t), \sigma(t)) \in \mathcal{Z} \,:\, \text{eq. (2) or eq. (3)}\}. \tag{12}$$

The aim then is to find all histories $(\epsilon(t), \sigma(t))$ in the intersection $\mathcal{D} \cap \mathcal{E}$, i. e., all histories that are admissible and satisfy the constitutive relations of the material.

Suppose, however, that the complex modulus $\mathbb{E}(\omega)$ of the brain tissue, and therefore its data set $\mathcal{D}$, eq. (11), is not known exactly but only approximately through empirical data in the frequency domain, e. g., resulting from *in situ* MRE. Under these conditions, the intersection $\mathcal{D} \cap \mathcal{E}$ is likely to be empty, i. e., there is no history $(\epsilon(t), \sigma(t))$ that is both admissible and in the material data set. Instead, we seek a pair of histories, an admissible history $(\epsilon'(t), \sigma'(t)) \in \mathcal{E}$ and a material history $(\epsilon''(t), \sigma''(t)) \in \mathcal{D}$, that are as close as possible to each other in the the sense of some suitable metric. Since, at steady state, the Fourier transforms $(\hat{\epsilon}(\omega), \hat{\sigma}(\omega))$ are Dirac deltas, the flat norm of measures suggests itself as a suitable metric. Indeed, we recall that the flat-norm distance between two Dirac deltas quantifies the discrepancy between both their amplitudes and points of application, as required.

The fixed-point iterative solver used in calculations is listed in Algorithm 1.

Algorithm 1 Data-driven solver, harmonic loading.

Require: Dynamic viscoelasticity data set $\mathcal{P} = \{(\omega, \mathbb{E})\}$, B-matrix, member weights W. Applied amplitudes F and G, applied frequency Ω, cutoff frequency ω_{cutoff}.

i) **Initialization**. Set $k = 0$. For all $e = 1, \ldots, m$, choose $(\omega_e^{(0)}, \mathbb{E}_e^{(0)})$ randomly from $\mathcal{P}$.

ii) **Displacement problem**. Solve for $U^{(k)}$ such that

$$B^T W \mathbb{E}^{(k)} (B U^{(k)} + G) - M \Omega^2 U^{(k)} = F, \tag{13}$$

iii) **Local states**. Compute

$$E^{(k)} = B U^{(k)} + G, \quad S^{(k)} = \mathbb{E}^{(k)} E^{(k)}. \tag{14}$$

iv) **Data assignment**. For all $e = 1, \ldots, m$,

iv.a) Find $(\omega_i, \mathbb{E}_i)$ in $\mathcal{P}$ s. t. $d(Z_e^{(k)} \delta_\Omega, \{S = \mathbb{E}_i E\} \delta_{\omega_i})$ is minimal.

iv.b) Set $(\omega_e^{(k+1)}, \mathbb{E}_e^{(k+1)}) = (\omega_i, \mathbb{E}_i)$

v) **Convergence test**.

if $\mathbb{E}^{(k+1)} = \mathbb{E}^{(k)}$, $U = U^{(k)}$, $E = E^{(k)}$, $S = S^{(k)}$, **exit**.

else, $k \leftarrow k + 1$, **goto** (ii).

Patient-specific models

For completeness, we report the histograms of the complex moduli in the material data sets, binned by voxel, for all eight patients considered in patient-specific calculations. We additionally report the computed contours of real and imaginary components of both maximum and minimum principal strain across the entire brain for all eight patients.

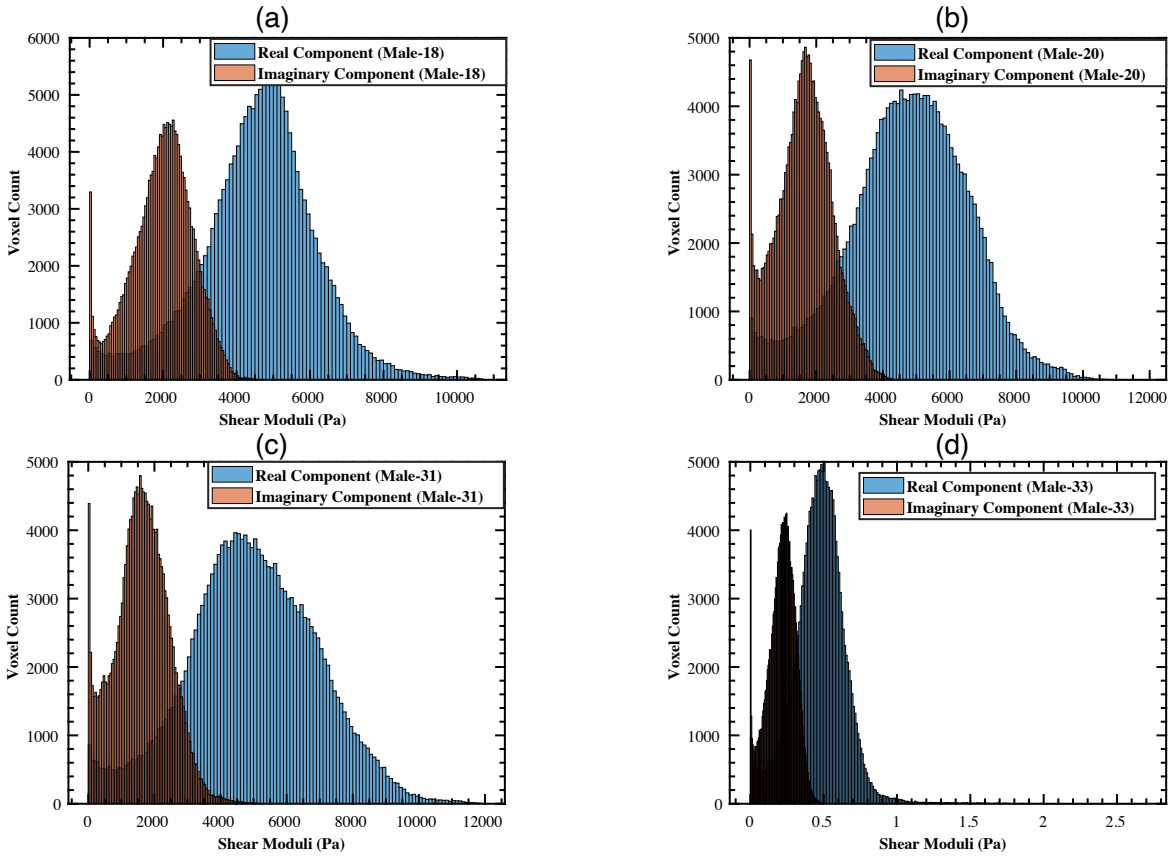

Fig. S1. Data-Driven (DD) brain mechanics allows for patient specific modeling: Histograms of complex shear moduli obtained from MRE data for four different male subjects used for corresponding DD models. Both the geometry and viscoelastic map are obtained from the publicly available MRE data provided by [9].

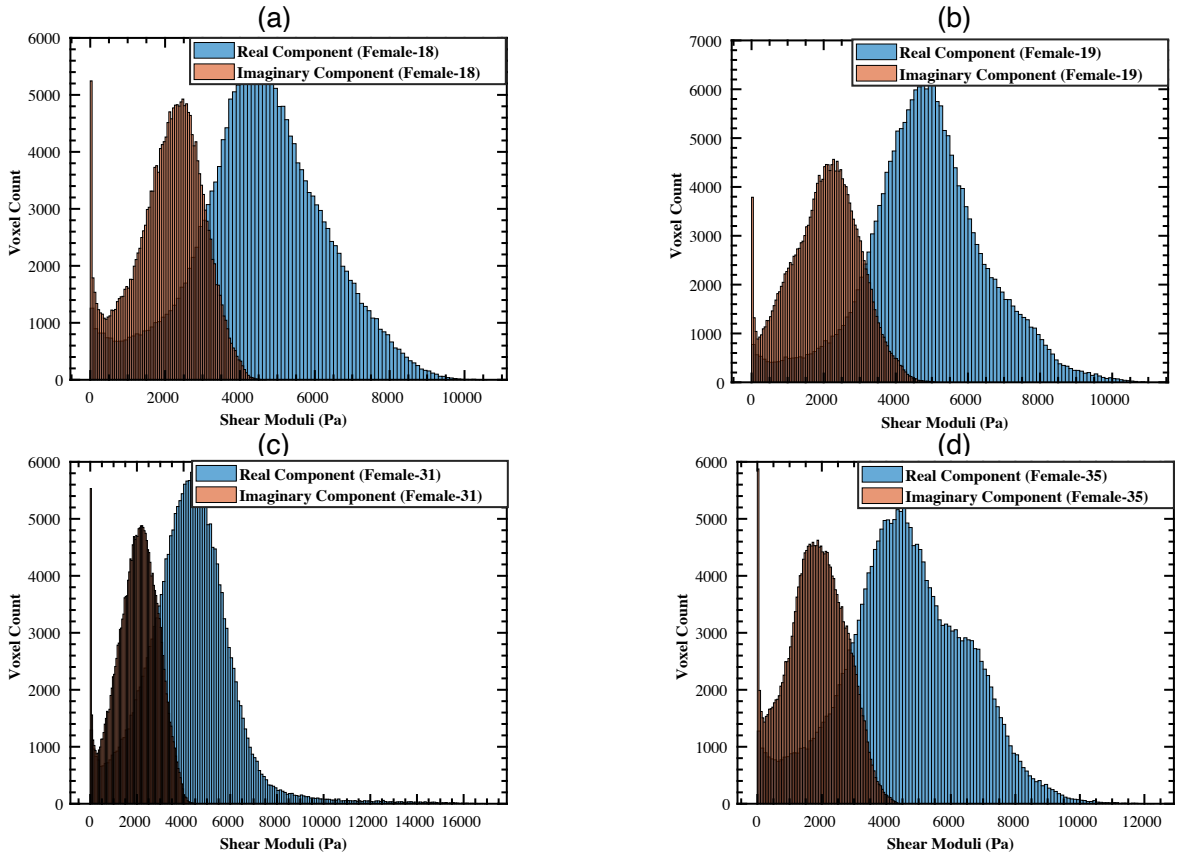

Fig. S2. Data-Driven (DD) brain mechanics allows for patient specific modeling: Histograms of complex shear moduli obtained from MRE data for four different female subjects used for corresponding DD models. Both the geometry and viscoelastic map are obtained from the publicly available MRE data provided by [9].

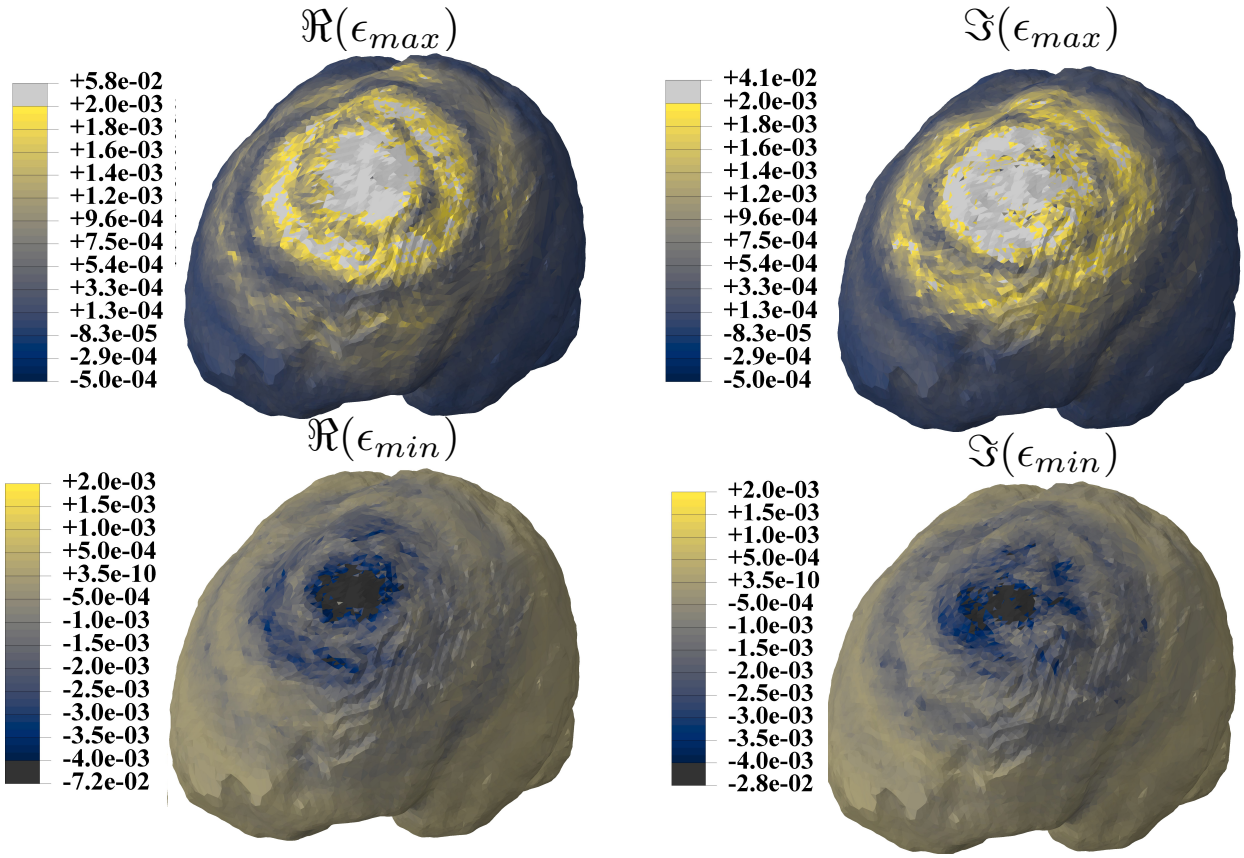

Fig. S3. Patient-specific model for 18 year old male subject: the real and imaginary components of maximum and minimum harmonic principal strain at 50 Hz, accumulated due to application of transcranial ultrasound on a region on the frontal lobe of brain.

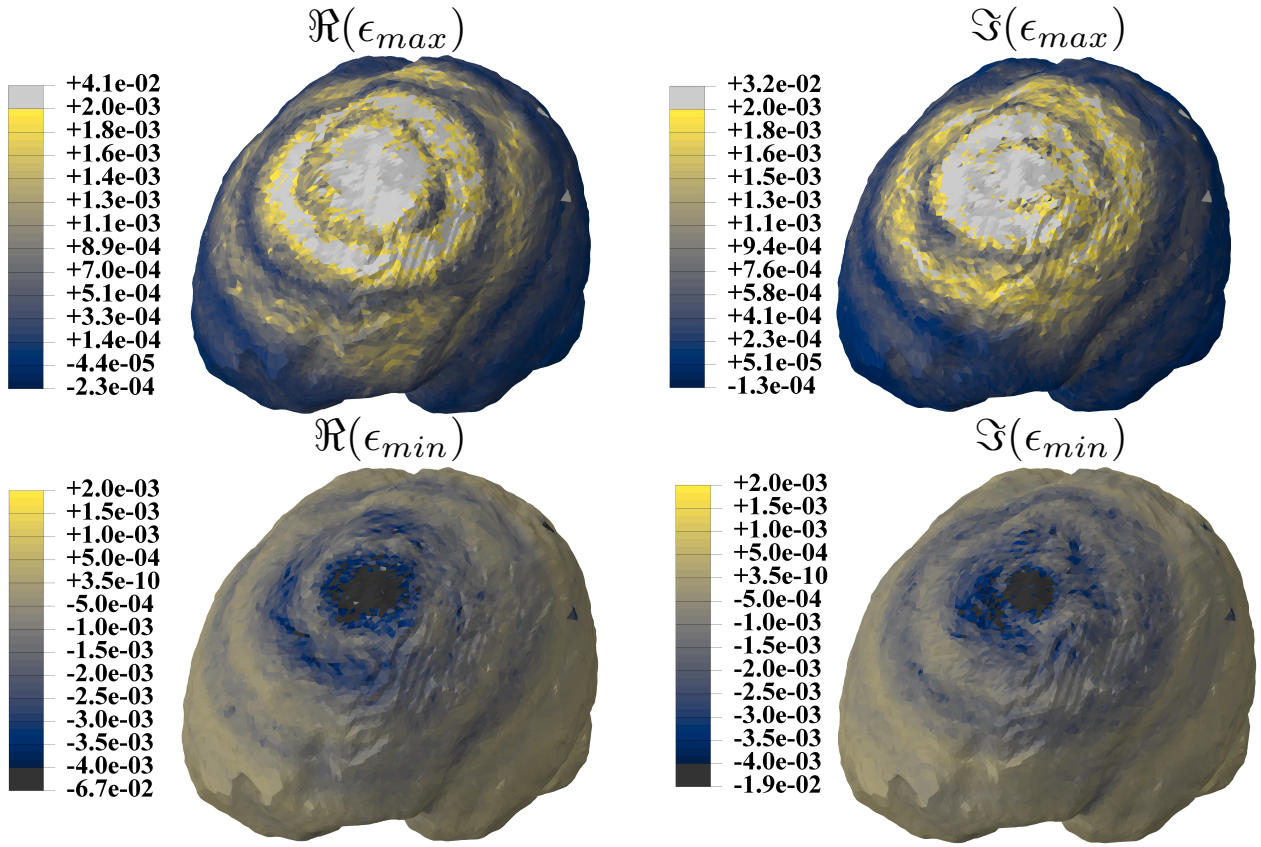

Fig. S4. Patient-specific model for a 20 year old male subject: the real and imaginary components of maximum and minimum harmonic principal strain at 50 Hz, accumulated due to application of transcranial ultrasound on a region on the frontal lobe of brain.

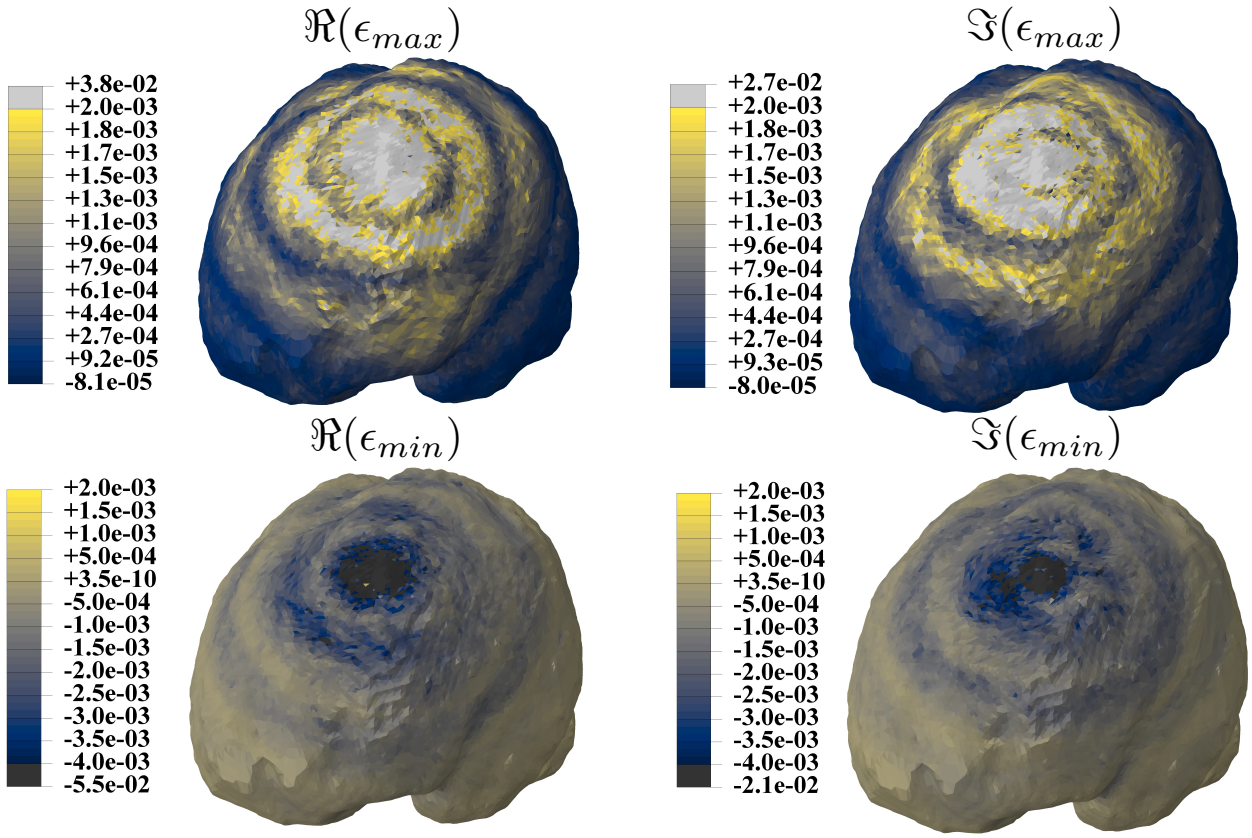

Fig. S5. Patient-specific model for a 31 year old male subject: the real and imaginary components of maximum and minimum harmonic principal strain at 50 Hz, accumulated due to application of transcranial ultrasound on a region on the frontal lobe of brain.

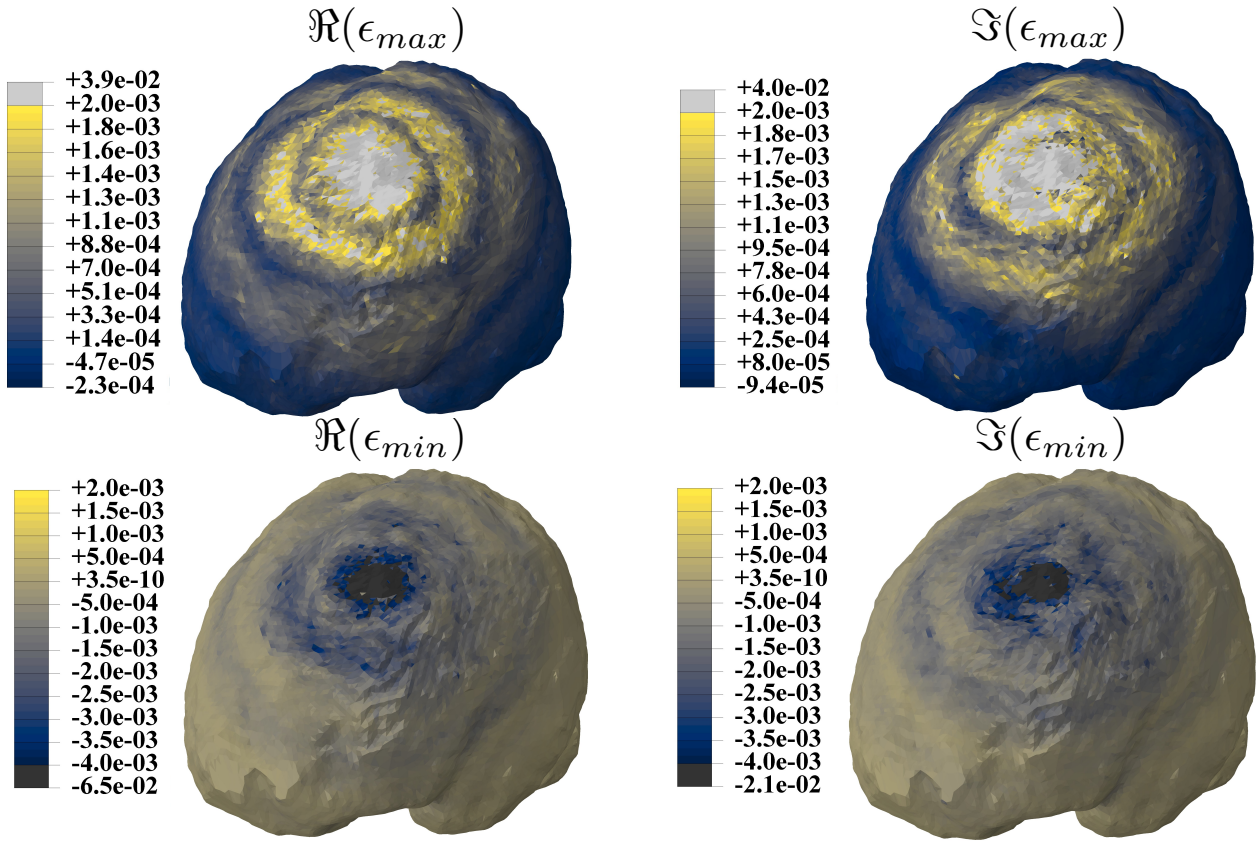

Fig. S6. Patient-specific model for a 33 year old male subject: the real and imaginary components of maximum and minimum harmonic principal strain at 50 Hz, accumulated due to application of transcranial ultrasound on a region on the frontal lobe of brain.

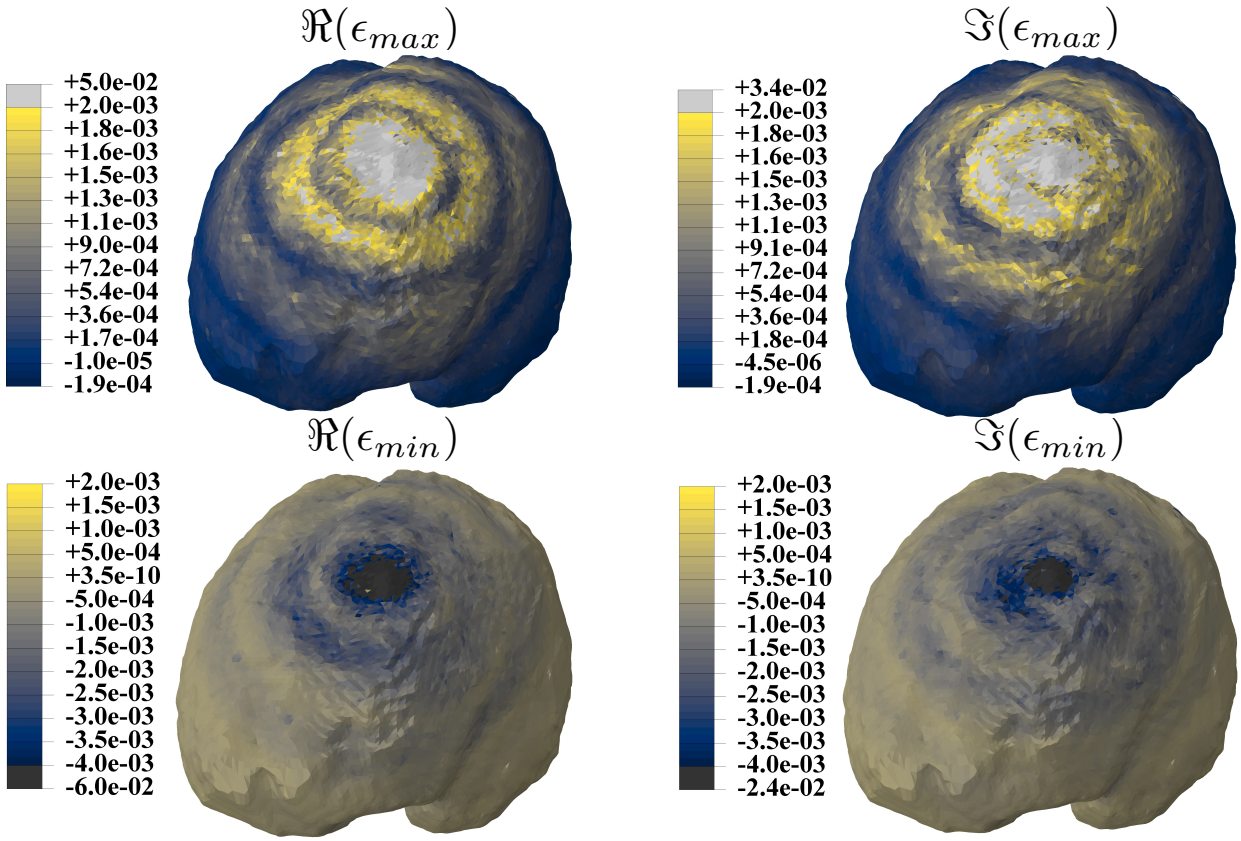

Fig. S7. Patient-specific model for a 19 year old female subject: the real and imaginary components of maximum and minimum harmonic principal strain at 50 Hz, accumulated due to application of transcranial ultrasound on a region on the frontal lobe of brain.

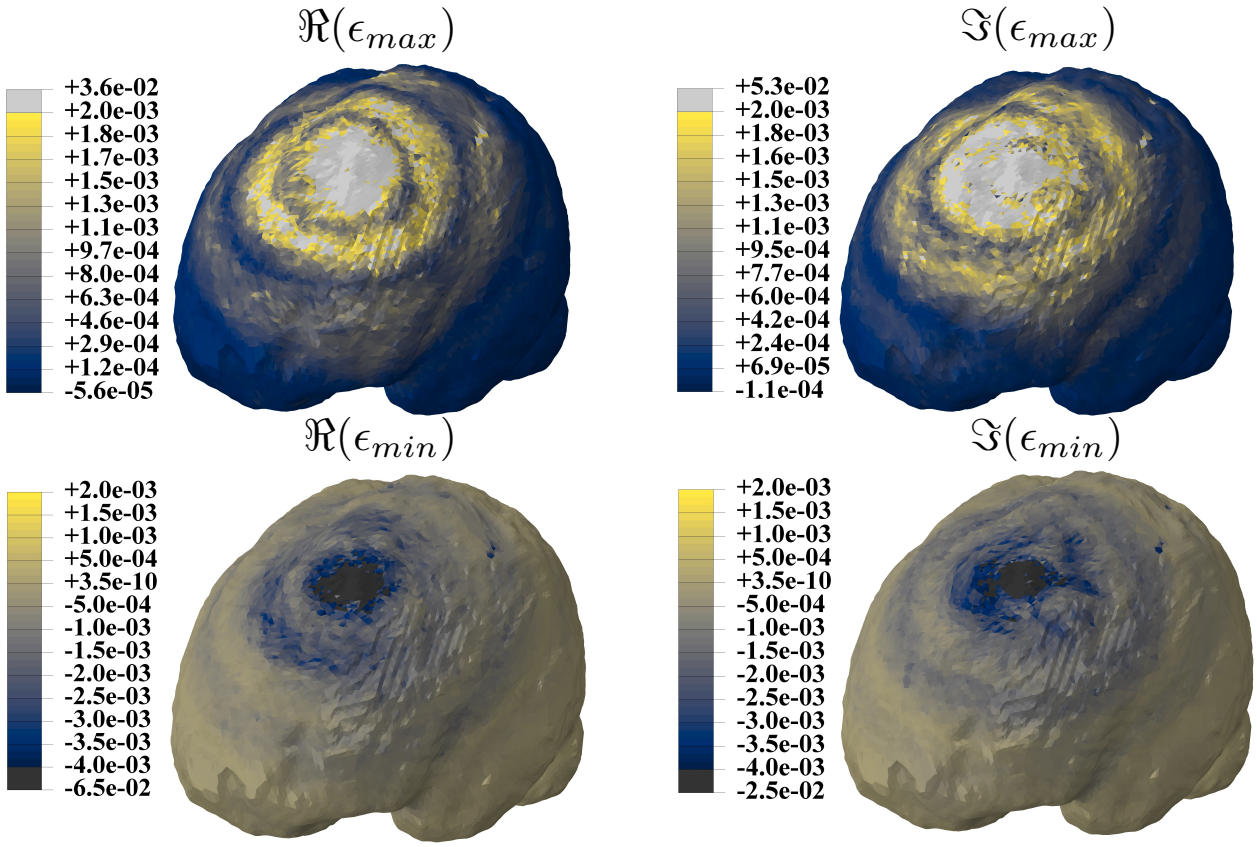

Fig. S8. Patient-specific model for a 18 year old female subject: the real and imaginary components of maximum and minimum harmonic principal strain at 50 Hz, accumulated due to application of transcranial ultrasound on a region on the frontal lobe of brain.

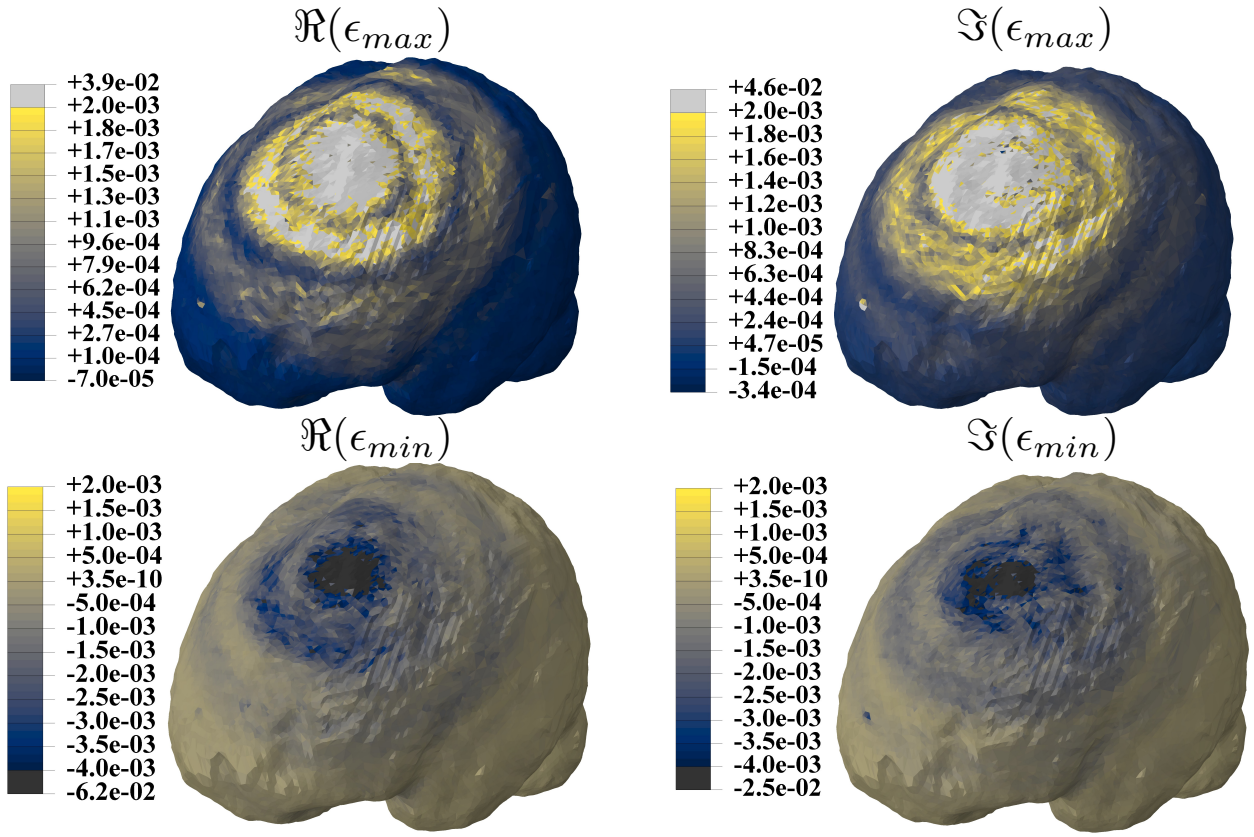

Fig. S9. Patient-specific model for a 31 year old female subject: the real and imaginary components of maximum and minimum harmonic principal strain at 50 Hz, accumulated due to application of transcranial ultrasound on a region on the frontal lobe of brain.

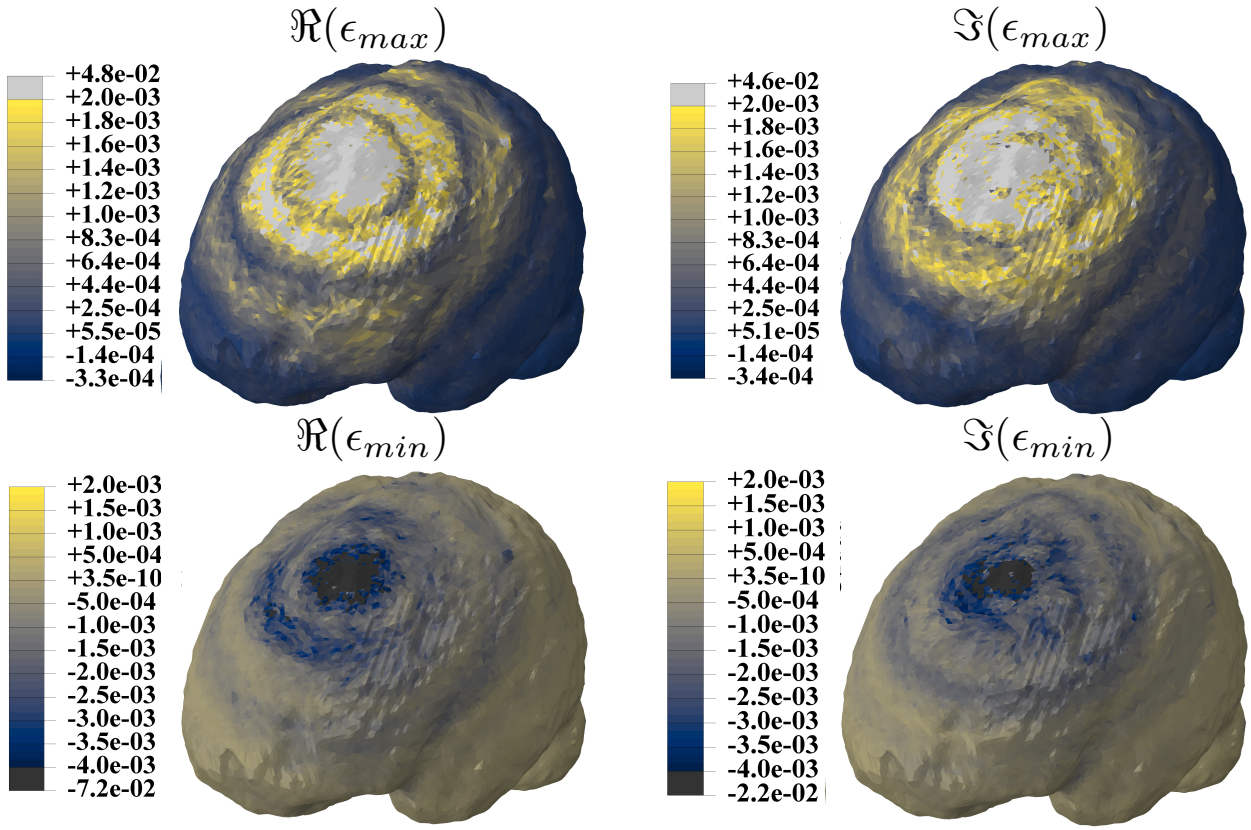

Fig. S10. Patient-specific model for a 35 year old female subject: the real and imaginary components of maximum and minimum harmonic principal strain at 50 Hz, accumulated due to application of transcranial ultrasound on a region on the frontal lobe of brain.